Available online at www.sciencedirect.com
ScienceDirect
Icarus 196 (2008) 78–89
ICARUS
www.elsevier.com/locate/icarus

Numerical assessment of the effects of topography and crustal thickness on martian seismograms using a coupled modal solution–spectral element method

C. Larmat [a,*], J.-P. Montagner [a], Y. Capdeville [a], W.B. Banerdt [b], P. Lognonné [c], J.-P. Vilotte [a]

[a] *Laboratoire de Sismologie Globale, IPGP Case 89, 4 Place Jussieu, 75252 Paris Cedex 05, France*
[b] *Jet Propulsion Laboratory, 4800 Oak Grove Drive, Pasadena, CA 91109, USA*
[c] *Laboratoire de Planétologie et Études Spatiales, IPGP, 4 Avenue Neptune, 94107 Saint Maur des Fossés, Saint-Maur, France*

Received 26 May 2006; revised 16 November 2007

Available online 19 March 2008

Abstract

The past 4 decades of Mars exploration have provided much information about the Mars surface, when its interior structure remains relatively poorly constrained. Today available data are compatible with a large range of model parameters. Seismology is able to provide valuable additional data but the number of seismographs will likely be quite limited, specially in the early-stage of future Mars seismic networks. It is thus of importance to be able to correctly isolate effects induced by the crust structure. Mars topography is characterized by spectacular reliefs like the Tharsis bulge or the Hellas basin and by the so-called "Mars dichotomy": the north hemisphere is made up of low-altitude plains above a relatively thin crust when the south hemisphere is characterized by a thick crust sustaining high reliefs. The aim of this paper is to study the effects induced on seismograms by the topography of the surface and crust–mantle discontinuities. Synthetic seismograms were computed using the coupled spectral element–modal solution method, which reduces the numerical cost by limiting the use of the spectral element method to the regions where lateral variations, like the presence of a topography, are considered. Due to numerical cost, this study is limited to long period and thus focuses on surface waves, mainly on long period Rayleigh waves. We show that reliefs like the Tharsis bulge or the Hellas basin can induce an apparent velocity anomaly up to 0.5% when only the surface topography is introduced. Apparent anomalies can raise up to 1.0% when the surface topography is fully compensated by a mirror-image topography of the crust–mantle discontinuity. Travel-time of surface wave are systematically increased for seismometers in the north hemisphere of Mars and decreased in the south hemisphere. When comparing effects on seismograms by the Earth and Mars topography, we found them to be larger for the Earth. It is due to the fact that we work with a seismic velocity model of Mars with a mean crust thickness of 110 km when the crust thickness has a mean value of 50 km for the Earth. When changing the Mars model for a thinner crust with a mean thickness of 50 km, effects by the topography on Mars seismograms becomes of the same order when not larger than what is observed on the Earth.

Keywords: Geophysics; Mars, surface; Earth

1. Introduction

40 years of martian missions have provided a good knowledge about the martian surface, such as about its topography, geology, meteorological conditions. On the contrary, seismology on Mars has been problematic. The Viking program (probes' launch in 1975—officially ended in 1983) included seismometers, but only the seismometer of Viking 2 was successfully deployed and fulfilled its reconnaissance task. However, it was insufficiently sensitive to record useful seismic signal, that latter been conspicuously mixed with noise due to the strong martian wind (Anderson et al., 1976, 1977). The French–Russian Optimism experiment (Lognonné et al., 1998) was lost in the failure of the launch of the Mars96 mission. The Netlander and Mars Premier projects revived the interest in the seismic study of Mars (Lognonné et al., 2000)

* Corresponding author. Fax: +33 1 44 7 38 94.
E-mail addresses: carene@lanl.gov, larmat@ipgp.jussieu.fr (C. Larmat).

0019-1035/$ – see front matter
doi:10.1016/j.icarus.2007.12.030

but were canceled in 2003. During the last decades, many studies have been carried out with the aim to prepare seismic missions on Mars. Technical aspects related to seismometers for Mars have been addressed in order to respond to the tough constraints of transport and installation (Harri et al., 1999; Lognonné et al., 2000). Some of the issues affecting a martian Network configuration have been addressed as well (Mocquet, 1999). The Geophysics and Environmental Package (GEP) module of the future European Aurora-ExoMars mission is planned to include a seismometer (Biele et al., 2007). The lander is planned to arrive on the surface of Mars in 2013.

The determination of the structure of a planet is the first step towards the understanding of the geodynamic processes which drove the formation and the evolution of that planet. From the Earth and the Moon, we know that seismology is one of the most efficient tool for gaining insight into the details of the internal structure of terrestrial planets (see Lognonné, 2005; Lognonné and Johnson, 2007, for a review). Travel-times of seismic waves traveling off internal discontinuities bring accurate constraints. Moreover, the distribution and occurrence of seismic events or seismic noise should provide information about the present rate of stress release and therefore about the stress state of the lithosphere. Seismology can thus play a fundamental role as a key component of a necessary multidisciplinary approach (Harri et al., 1999) in order to determine the deep structure of Mars (Verhoeven et al., 2005). In the future, by comparing the structures of several planets, the scenarios of the formation and the evolution of the Earth and our Solar System will be better understood.

The crust of Mars exhibits several distinctive features such as topography elevations ranging over 27 km and the existence of a marked crustal dichotomy (Zhong and Zuber, 2001). We thus expect that the biases in seismograms induced by the surface topography and the shallow structure down to the base of the crust might be more significant than on the Earth. Moreover, the likely limited number of seismic stations in the early-stage of the future Mars seismic network (for example, only one seismometer will be deployed by ExoMars and all attempt in the past for deploying a network has been canceled due to lack of funding) makes the correct interpretation of seismograms more crucial. The purpose of this study is to evaluate and understand the effects of the lateral variation of topography and of thickness of the crust in order to optimize the determination of the deep structure of Mars from seismic information. Because our study is limited to long period, it is focused on surface waves and more specifically on Rayleigh waves which might be used for internal studies, including on the crustal thickness, even when only one instrument is used (Lognonné and Johnson, 2007). In a first section, we outline the known constraints upon the seismicity and the structure of Mars crust. Then, the numerical method used in this study is briefly introduced. Results of our modeling are presented in the following section. Finally, we draw some conclusions in the last section.

2. A strongly heterogeneous subsurface structure with significant topography

2.1. Description of the lateral heterogeneity of the martian crust

Mars topography has been determined by measurements of the Mariner 9 and Viking Orbiter occultations (Smith and Zuber, 1996) and since then from the data provided by the Mars Orbiter Laser Altimeter (MOLA) (Smith et al., 2001). Mars topography exhibits spectacular values: Olympus Mons stands over the surrounding plains by about 20 km and the Hellas impact basin is more than 8 km deep, which makes the topographic range of Mars the largest of the Solar System. Fig. 1 shows the distribution of the topography and the crustal thickness for both Mars and the Earth. The global Digital Elevation Models (DEM) used are the MOLA topographic model with a sampling of $1^\circ \times 1^\circ$ for Mars and a coarse version of the model Global 30 Arc Second Elevation Data (gtopo30) with a sampling of $0.5^\circ \times 0.5^\circ$ for the Earth. The model of Mars crust thickness is a spherical development up to the degree 50 developed by Zuber et al. (2000) when assuming an average crust density of 2900 $\mathrm{kg\,m^{-3}}$. The crust thickness of the Earth comes from the 3-Dimensional Seismological Model A Priori Constrained (3SMAC; Ricard et al., 1996). These topography and crustal thickness models will be used throughout this whole study. From those data, the Mars topography extends from -0.22 to 0.61% relatively to the planet's radius whereas the Earth topography ranges from -0.15 to 0.09%; these peak values naturally depend on the spatial sampling of the models, as coarser sampling rates tend to average out extrema.

The second remarkable feature which can be seen in Fig. 1 is the crustal dichotomy of Mars. The crust of the southern hemisphere is thick, with numerous impact craters, whereas the crust of the northern hemisphere has a young surface and is relatively thin. The crustal dichotomy might be a consequence of a one-degree mantle convection (Zhong and Zuber, 2001). The existence of a thick, weak asthenosphere early in Mars history, which is supported by models of the thermal evolution of the martian lithosphere (Zuber et al., 2000), would favor this mode of long-wavelength convection.

Finally, the distributions of topography and crustal thickness correlate well to each other for Mars. This reflects the fact that the martian topography is highly compensated but at greater depths compared to the Earth, where both resurfacing and tectonics are much more active.

2.2. Constraints on a seismic velocity model for Mars: The inversion problem

Inversion of the deep structure of Mars is highly non-unique since strong assumptions are required, such as the mean depths and densities of the major divisions or the distribution of major elements (Mocquet et al., 1996). Thus different studies came up with different accounts upon the internal structure of Mars depending upon their working hypothesis and the inverted data. The recent determination of the k_2 gravity Love number by

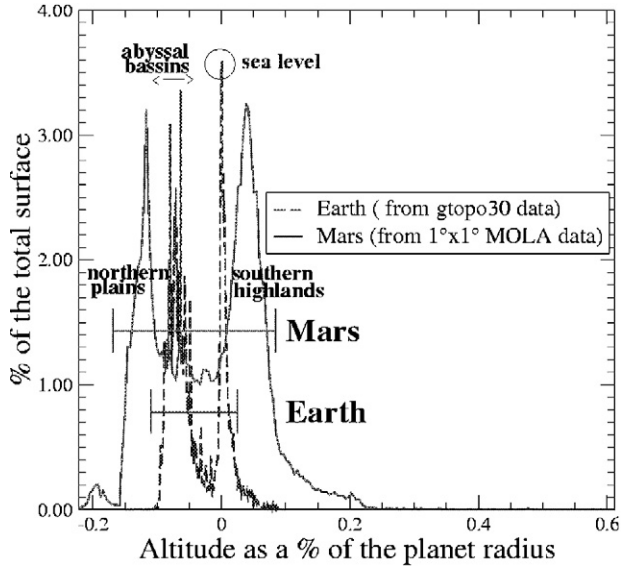

(a)

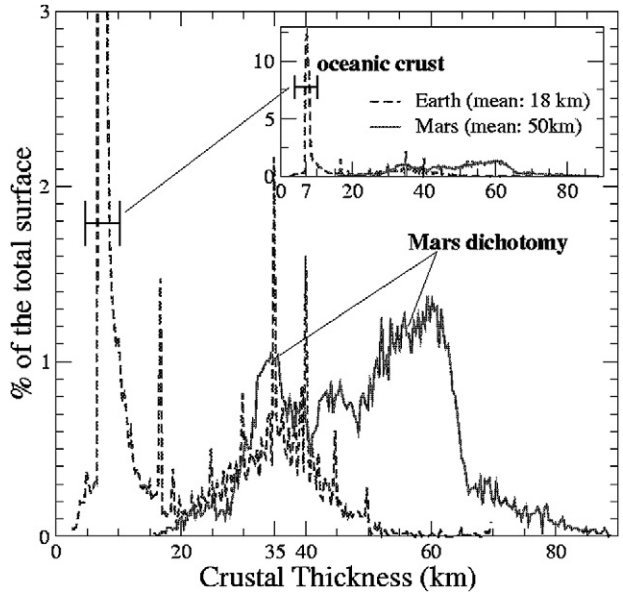

(b)

Fig. 1. (a) Hypsometric curves for the martian and the terrestrial topography models (see details in text) when elevations are expressed as a percentage of the radius of the planet and are distributed into 200 bins. The erosion by water dominates the terrestrial relief (see the single dominant peak at the sea level) whereas Mars topography curves displays two dominant peaks which correspond to the dichotomy of the Mars crust between the southern and the northern hemisphere. Overall Mars exhibits a larger topographic range than the Earth. (b) Distribution (into 200 bins) of the crustal thickness of Mars and Earth. For this later, about 45% of the crust is of oceanic nature and corresponds to a thickness ranging from 6.3 to 8.4 km. By contrast, the thickness of the continental crust is quite irregularly scattered between 20 and 50 km. Mars exhibits a simpler bimodal distribution, well correlated with the topography bimodal distribution.

Yoder et al. (2003) implies a liquid iron core with a radius from 1520 to 1820 km. Joint inversion by Spohn et al. (1998) of geophysical and geochemical data (moment of inertia, gravity and bulk composition from chondritic meteorite) has lead to an estimation for the core radius of 1468 and 1667 km, respectively for the two end-member models they proposed. A liquid core has also been suggested by Lognonné and Mosser (1993), based on the interpretation of the Phobos secular attenuation and inferred martian Q value. In those models, the velocities increase linearly within the layers composing the crust and the mantle and parabolically in the liquid core (no solid core). The velocity gradient is smaller than in the Earth because of the smaller pressure gradient. Therefore, Mars is expected to be less dispersive than the Earth for surface waves, and R1 and R2 should therefore have a larger and more impulsive waveform than on Earth.

As for the thickness and the mean density of the crust and of the lithosphere, they have more specifically been determined by the degree of differentiation of the planet during its formation and the entire following magmatic building of the crustal material. This latter is directly related to the vigor of the mantle convection and to the concentration of heat producing elements such as P, K or U. Different data are available to gain insight into those processes which have driven the crust formation: SNC meteorites have been used to constrain the bulk composition; knowledge about the mass distribution within Mars comes from estimations of the moment of inertia (Sohl and Spohn, 1997; Spohn et al., 1998); Geoid-to-Topography Ratios (GTRs) have been derived from the measurements of orbiting probes such as Mars Global Surveyor (Malin and Edgett, 2001) and provide information about the stresses distribution within the lithosphere (Banerdt, 1986; Turcotte et al., 2002; Belleguic et al., 2005); models of viscous relaxation of topographic features such as the Tharsis buldge provide also information about the state and age of the lithosphere (Zuber et al., 2000; Nimmo and Stevenson, 2001); in situ measurements of the concentration of some radiogenic elements allow mass-balance computation in order to estimate the volume (and thus the thickness) of the crust as a geochemical sequestration reservoir (McLennan, 2001). The conservative range for Mars crust densities is from 2700 to 3100 kg m^{-3}, densities displayed by rocks within the lower crust of the Earth. Belleguic et al. (2005) found a higher density of about 3200 kg m^{-3} beneath the Elysium rise volcanic region. Wieczorek and Zuber (2004) made a critical review of different recent studies about the Mars crust thickness. They advocate for a lower bound of 32 km (Zuber et al., 2000; Wieczorek and Zuber, 2004) and an upper limit of 100 km (Nimmo and Stevenson, 2001) for the mean of crust thickness. This later in the two end-member models proposed by Sohl and Spohn (1997) and Spohn et al. (1998) are respectively of 100 and 250 km. In situ future measurements of the geochemical composition of the crust material and of seismic wave travel-time are required in order to constrain the current estimations.

In this study, all our seismograms are computed with the first conservative velocity model proposed by Sohl and Spohn (1997) and Spohn et al. (1998) (model A). That model presented in Fig. 2 (solid curve) is optimized to satisfy the estimated moment of inertia of Mars. The crust has a mean thickness of 110 km, the density is of 2800 kg m^{-3}, the P travel velocity of 7.66 m s^{-1} and the S travel velocity of 4.03 m s^{-1}. Note that our results are not strongly sensitive to densities but mainly to seismic velocities and thicknesses. Although the sur-

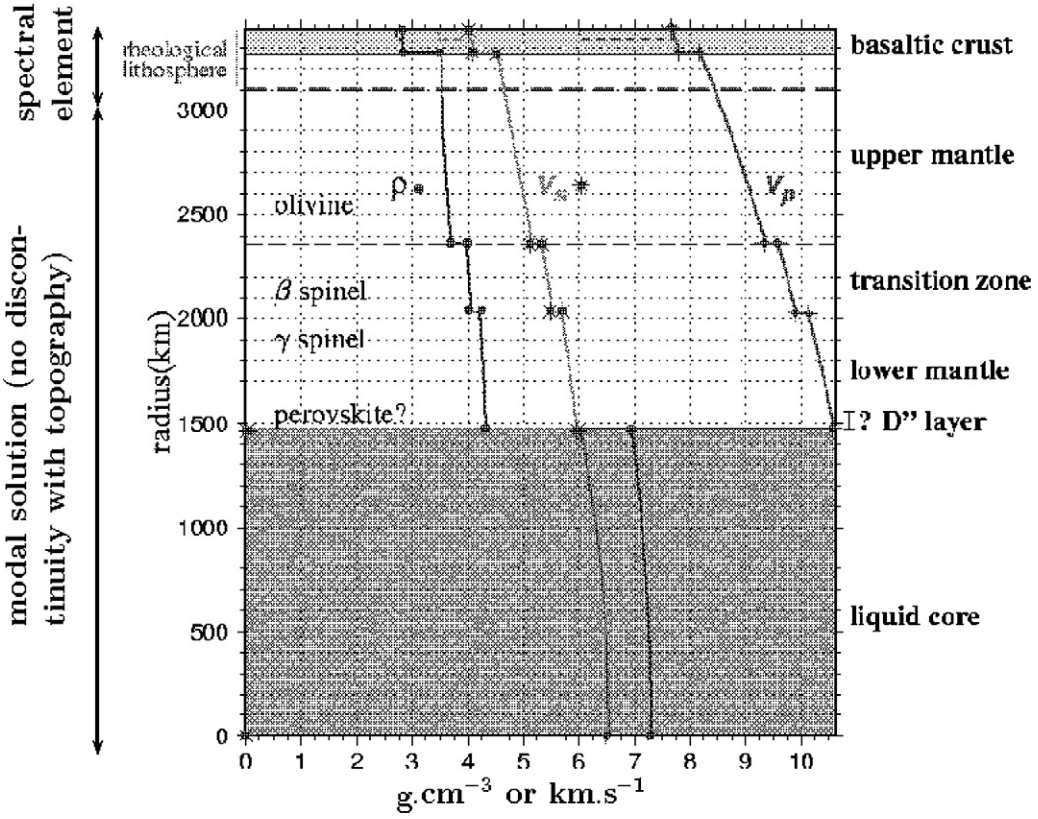

Fig. 2. (Solid line) Seismic velocity model proposed for Mars by Sohl and Spohn (1997) and by Spohn et al. (1998). Seismograms of Sections 4.1 and 4.2 were computed with this model when simple Gaussian topography have been introduced for the surface and the crust–mantle discontinuity ("Moho"). (Dashed line) Seismic velocity model of Mars used for Section 4.3 when an additional layer with a thickness of 50 km corresponding to an upper crust has been implemented.

face of Mars is enriched in iron (dense material), the above values are significantly higher than the ones commonly observed at the surface of the Earth and may have been biased by an insufficient sensitivity of the data to the thinner upper part of the crust and the lack of additional in situ information. We have thus chosen to divide the crust into two 50 km thick layers. In the lower part, we have kept the values of the above model while for the upper layer we have chosen a density of 2.7 kg m^{-3}, a velocity of 6.0 km s^{-1} for the P waves and of 3.46 km s^{-1} for the S waves (see Fig. 2, dashed line). Those values correspond to the terrestrial basaltic upper crust.

The seismic attenuation of Mars is constrained by the Phobos tide and may be intermediate between the Earth's upper mantle and lower mantle one (Lognonné and Mosser, 1993; Zharkov and Gudkova, 1997) with a value for Q around 200 at periods around 100 s. This value conforms with recent studies (Yoder et al., 2003; Bills et al., 2005) which suggest a Q around 100 at the Phobos rotation frequency, assuming a frequency dependence law like $Q \propto f^{0.15}$ discussed in Lognonné and Mosser (1993). Although attenuation might lead to significant amplitude attenuation, as already studied by Lognonné et al. (1996), our study is focused on the amplitudes of R1 and R2, which correspond to a much smaller ratio between the propagation path and the wavelength (a path of one wavelength corresponds to a full cycle for the factor quality). We thus neglect this effect in this study and chose to focus on the effect of topography.

2.3. Present constraints on the martian seismicity

Meteorite impacts and tectonics sustained by the cooling of the lithosphere are expected to be the natural sources of Marsquakes. By quantifying the moment release of visible faults and estimating their ages using stratigraphic scales, the current moment release for the whole lithosphere can be estimated. This total moment is shared within a distribution of seismic events by assuming a relationship between the size and the occurrence rate of seismic events. Calibration of this method has been done versus the seismicity of the Moon (Golombek et al., 1992; Golombek, 2002). Mars is expected to be less active than the Earth but more active than the Moon. About fourteen globally detectable events (i.e., $M_b \geqslant 4$) are expected per year.

Only one seismic experiment performed by the Viking 2 mission has been achieved so far on Mars (Anderson et al., 1976). But the record did not provide a conclusive detection of a martian seismic event because of the low resolution of the instrument and a high sensibility to the wind enhanced by the fact that the seismometer was fastened to the lander. One Marsquake is suspected on Sol80 but was not undeniably proved (Anderson et al., 1977).

The sources in our simulations are explosions of 10^{18} N m. This corresponds to a moment release of $Mw = 5.9$ according to the Kanamori law (assuming a stress drop of about 30 bars) and might be the largest magnitude event which could be detected during a 2 years operation. This chosen value for the

magnitude corresponds to middle-size earthquakes. Because of a limitation of computational resources, the period range we worked with was from 80 up to 500 s. This long period range is not optimal for the study of the effects on seismograms by the finest details of the crust structure, such as the possible diffraction induced by the mega-regolith layer. This study focuses on the influence of large features like the Tharsis bulge, the Hellas basin or the south–north dichotomy of the crustal thickness.

3. The numerical method: The coupled modal solution–spectral element method

This study is an application of a recently developed numerical method which couples a solving scheme based on spectral element with a modal solution (Capdeville, 2000; Capdeville et al., 2003). The physical domain is divided into two parts (see Fig. 2). Only the outermost part is discretized by the spectral element method while the propagation in the inner region is introduced via a dynamic boundary condition on the interface between the two parts. That boundary condition is calculated using an operator developed in the spherical harmonics basis. Thus, the method joins the accuracy of the spectral element method (SEM) for heterogeneous media (Komatitsch, 1997) with the low computational cost of the modal solution. The domain discretized by the modal solution is spherically symmetric (no coupling between the eigenfunctions), which is an acceptable assumption even for the Earth since the resolution upon lateral variations from broad-band records decreases in these parts. The coupling is more precisely outlined in Capdeville et al. (2002, 2003). The design of a mesh for the spectral element method comes from the adaptation of the mesh "cubed sphere" for a three-dimensional spherical model of a planet with seismic discontinuities (Chaljub, 2000; Chaljub et al., 2003). That mesh is made up from hexahedra.

As in any finite elements method, the quality of the discretization of the media depends on the number and on the shape of the elements. For the spectral element method, the shape of an element is uniquely defined by the transformation function from a reference element of the same topology class (i.e., the unit cube for an hexahedra) to the considered element. For models with spherical symmetry, analytical transformations are available (Chaljub, 2000; Chaljub et al., 2003). When the modeled system is of random shape, like a planet with a given topography, we have to use parametric transformations for which the transformation of a given element (transformation denoted by $\mathcal{F}_e$) is given by a set of n_a points of the modeled space associated with the "shape functions" $\mathcal{N}_a$. In this case: $\mathbf{r}_e(\xi,\eta,\gamma) = \mathcal{F}_e(\xi,\eta,\gamma) = \sum_{a=1}^{n_a} \mathcal{N}_a(\xi,\eta,\gamma)\mathbf{r}_a$, where (ξ,η,γ) are the Cartesian coordinates in the reference element, n_a denotes the number of control points, $\mathbf{r}_a$ is the position in the medium of the control point a, and $\mathbf{r}_e$ the position of any point in the element e. We use the Lagrange polynomials associated with the control points as shape functions. Each polynomial has the value 1 at its associated point and 0 at any other point, the degree of the polynomial functions is $n_a - 1$.

Note that topography is introduced through the finite set r_a, control points positions and is approximated by a polynomial function at any point which is not a control point. Therefore, only a smoothed version of the topography model can be introduced in the numerical method. In order to correctly truncate the actual intricate topography, we have chosen to use a finite spherical harmonic expansion to develop the given spatial function expressing the altitude of the control points. The cut-off degree can be selected according to a purely numerical criteria such as the mean size of the elements since the topographic spectrum is approximately self-affine (Turcotte, 1987).

In this study, since only the topography of the surface and of the crust–mantle discontinuity (termed "Moho") are considered, only the upper part of Mars needs to be discretized by spectral element. We chose the seismic discontinuity of order 1 at the depth of 482 km in Sohl and Spohn (1997) (corresponding to the end of the thermal lithosphere) to be the coupling interface between the modal solution and the spectral element method. That discontinuity is deep enough with respect to the "Moho" to consider that the surface topography is completely compensated at this depth, therefore all seismic discontinuities below can be considered without any topography.

4. Results: Numerical synthetic seismograms; comparison for Mars and Earth

After the implementation of topography in the SEM, we first try to identify the effects of topography in case of simple Gaussian reliefs. For these simple configurations, the velocity model is the model A proposed in (Sohl and Spohn, 1997; Spohn et al., 1998). The upper part of the model is deformed in order to introduce the topography of the surface and of the "Moho." Using these results for guidance, we have performed simulations in as much realistic models as possible for Mars with an additional layer mimicking an upper crust (see Fig. 2). Finally, we have compared the relative importance of these effects for Mars and the Earth.

Because our computations are at long periods (above 80 s), the seismograms presented in the following are dominated by surface waves (seismic sources typically radiate more body wave energy in short periods). Two types of seismic surface wave can be observed, Rayleigh waves which are a combination of vertical and longitudinal motions (resulting from the coupling of P and SV wave) and Love waves which include only pure transverse horizontal motion (guided SH wave). The first train of Rayleigh wave diverging from the source and converging at the antipode is termed "R1" when the following train diverging from the antipode is termed "R2." We recall that the seismic sources are explosions in order to introduce no polarity effect in this study.

4.1. The behavior of waves in the presence of simple topographic features

There has been little investigation of the effects of topography on seismic waves because they are usually considered less important than the effects of the local heterogeneities and of the layer structure of the propagation medium (Paolucci et al., 1999). Typically, when seismologists work with body wave

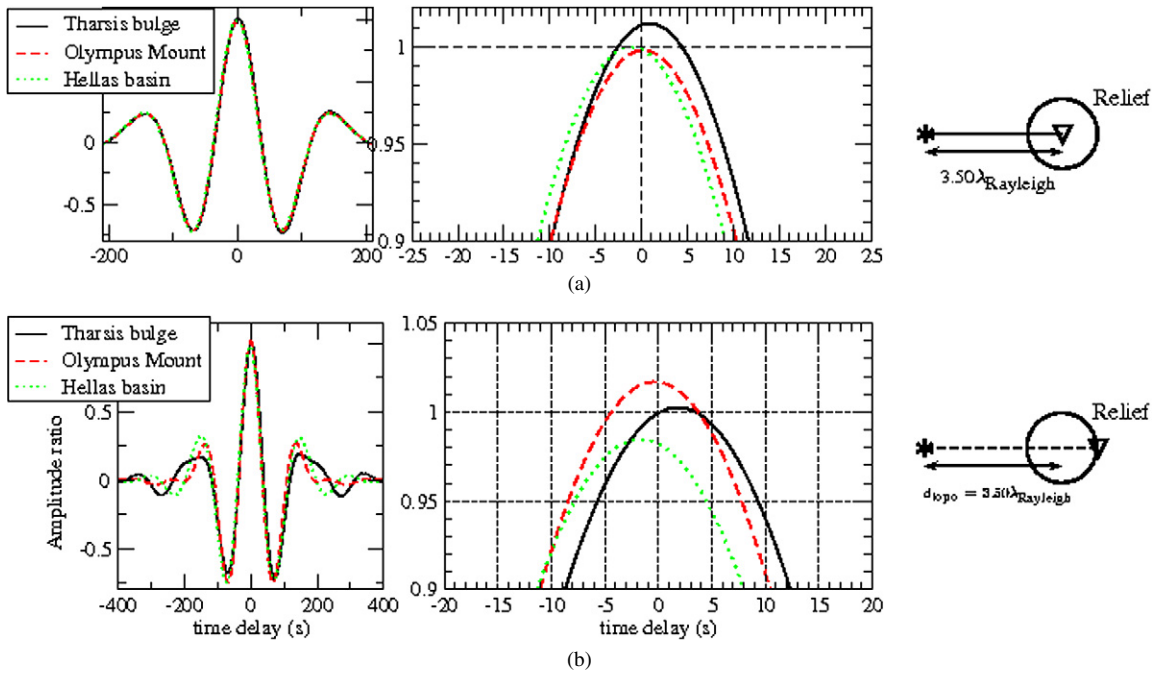

Fig. 3. Correlation over the first Rayleigh train arrival (R1) between synthetic seismograms computed in the presence of a Gaussian topography and corresponding seismograms computed when the surface has no topography. The Gaussian reliefs mimic real martian features (see Table 1). (a) Effects on the receiver at the center of the reliefs. The Tharsis bulge induces a time delay up to 1 s and an increase of the amplitude of 1%. As for the waves which have traveled across the Hellas basin, they display an advance of 1 s. Due to its small width, Olympus Mount does not introduce any time shift neither an amplitude change for a receiver at its summit. (b) Effects on the receiver at the edge of each Gaussian reliefs in the "forward" direction. The effects are much larger than in (a) in all cases.

Table 1
Parameters of the Gaussian reliefs fitting as well as possible 3 well-known features of the martian topography: Tharsis bulge, Olympus Mount, and Hellas basin

	h_0 (km)	b	n
Tharsis bulge	8	25°	2
Olympus Mount	20	4.2°	1
Hellas impact basin	−6	18°	3

The equation of the Gaussian is: $h(\theta,\phi) = h_0 e^{-(\frac{\Delta(\theta,\phi)}{b})^{2n}}$, where $\Delta(\theta,\phi)$ is the distance between the point of latitude θ and of longitude ϕ and the center of the relief. Larger is the degree of the Gaussian (n), sharper is the edge of the relief.

travel times, very simple corrections for topographic effects are performed. But these corrections are no longer valid when broadband seismic waveforms are considered.

First, we have performed simulations in simple configurations. We have considered a spherical model of Mars (Spohn et al., 1998) with a single mountain or crater of Gaussian shape, which fits as best as possible a real feature of the martian topography (see the relief parameters in Table 1). For the shape functions in the spectral element method, we have chosen to work with polynomials of degree 8 (meaning 9 control points in each direction) in order to fit as best as possible the Gaussian shape. The source point is at epicentral distance of 48.19° from the center of the relief and at a depth of 30 km. Note that this depth is much smaller than the typically determined source depth of tectonic events on the Moon (Lognonné et al., 2003). The source time function is a Ricker wavelet (second derivative of a Gaussian function) with a dominant period of 200 s.

Fig. 3 shows the cross-correlation of seismograms computed when the Gaussian reliefs are present with seismograms computed when no topography is considered; these latter are computed by a modes summation method. We can see that wide elevations in the relief (like the Tharsis bulge) tend to slow down seismic waves, when wide depressions (like the Hellas basin) accelerate them. Consequently the amplitude of the vertical component is increased by positive topography and decreased in the opposite case (up to 2% for Tharsis region and Hellas basin). When considering receivers at different source–receiver distances, we can observe that the topography effect on the seismograms is especially large within a range of one up to two wavelengths from the relief but never vanishes completely even at far distance. On the contrary, for the far narrower relief mimicking the Olympus Mount, no effects are visible in the forward direction for receivers at a distance greater than 5° from the edge of the volcan. This fact suggests a healing process of the wavefront as the one observed in the presence of scatterers.

The time delay can be up to 3 s for the whole R1 wavetrain. If that time-shift was interpreted as an accumulative effect of upper mantle heterogeneities, it would lead to an apparent anomaly of the order of 0.5% for a phase velocity of 4.51 km s^{-1}. Notice that it is only an estimation because a rigorous phase travel velocity analysis requires that the signal is decomposed into the different propagating surface wave modes. This is not done here.

When the extent of the topography is of the order of the dominant wavelength, new phases corresponding to diffracted waves can be observed on the seismograms presented in Fig. 4.

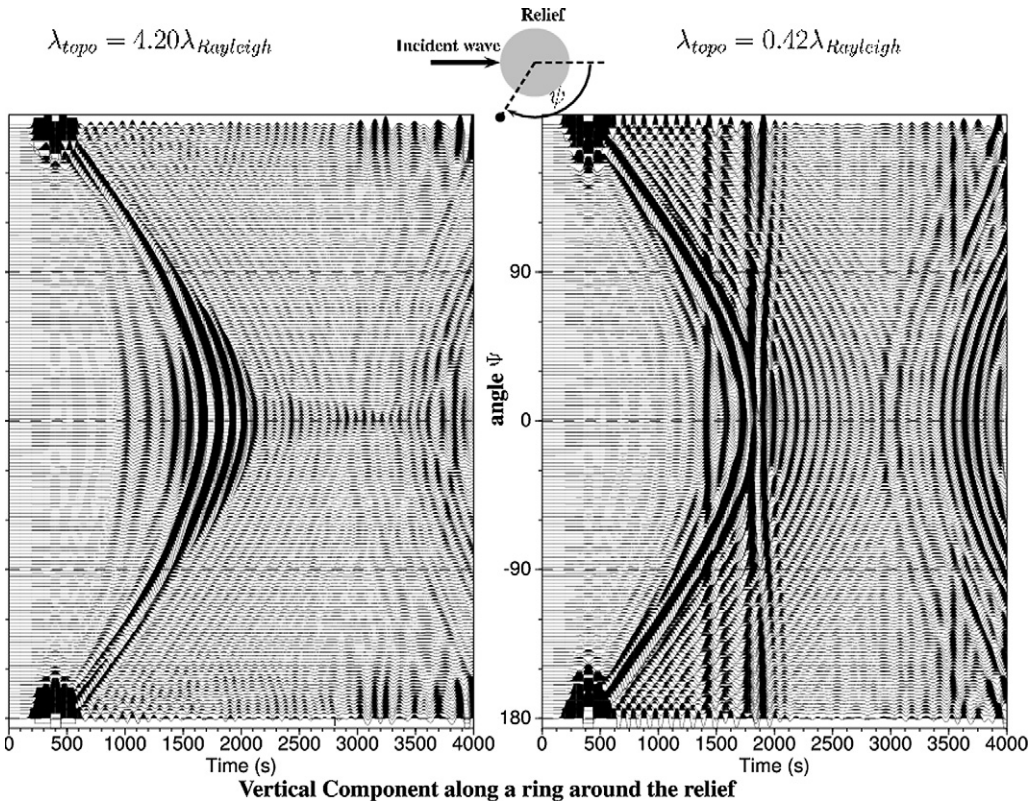

Fig. 4. Seismic signal produced by a Gaussian mountain displayed according to the ratio between its width and the dominant wavelength of the wave field. The seismic signal produced by the presence of the relief is extracted by making the difference of the seismogram computed with the mountain with the seismogram computed when there is no topography. These differential seismograms are ordered according to the diffraction angle Ψ (see inset). When the Gaussian mountain is wide (on the left), it mainly generates signal in the forward direction and thus can only be detected if the mountain is between the source and the receiver. When the mountain is narrow (on the right), it generates a strong diffracted signal in all direction.

4.2. The effect of a crustal root on the seismic signal

When the surface topography is fully compensated (isostasy), the crust–mantle discontinuity ("Moho") displays a topography which is proportional to the mirror image of the surface topography: mountains are thus supported by a thickening of the lighter crust ("roots") over the denser upper mantle; conversely a thinning of the crust is observed below basins. When introducing a compensating topography of the "Moho," the effects of the surface topography is larger on seismic waves (see Fig. 5). This is in agreement with the results of Snieder (1986). For this computation, we used two mountains with an extreme maximum height of 50 km at their summit in order to make the effects more obvious. We find time delays up to 50 s, which will lead to a velocity anomaly of 7.7% for a phase velocity evaluated at 4.52 km s^{-1}. With a height of 8 km, Tharsis could thus induce an apparent anomaly of more than 1% if it is fully compensated or down to 0.5% without a root as shown in the previous section.

4.3. Models with real topography for Mars and the Earth

For the two planets, we have performed simulations using realistic models for the surface topography and for the "Moho." The source time function of explosions is still a Ricker wavelet with a dominant frequency of 5 mHz (200 s) corresponding to a lower period of 80 s.

In Fig. 6, we present the synthetics for two great circles across an oceanic and a continental region for the Earth and the northern and southern hemispheres for Mars. For the models of Mars and the Earth used in this study, the crust is homogeneous; the only investigated variations are geometrical (thin or thick crust). The deformation of the signal is estimated by a time delay and an amplitude gain calculated for the whole signal without any filtering in the frequency domain. These quantities are presented as a function of epicentral distance in Fig. 7. The experiments clearly show a systematic behavior: traveling through a thin (/thick) crust, surface waves accumulate an advance (/delay, respectively). Notice that those geometrical effects would be amplified by lateral variations of the wave velocity if, for example, the thinner crust is made up of a denser material as it is the case for the oceanic crust of the Earth. For Mars, it is still not clear if the apparent crustal dichotomy implies a different composition of the crust in the south and in the north hemisphere (Belleguic et al., 2005).

For these experiments, the effects are surprisingly more important on the Earth than for Mars. This is most likely due to the fact that the "Moho" interface is far deeper in the second case. The thickness of the Earth crust varies from 5 to 374% relatively to its mean value, whereas the Mars crust thickness varies only from 69 to 136% relatively to its mean value (110 km). In or-

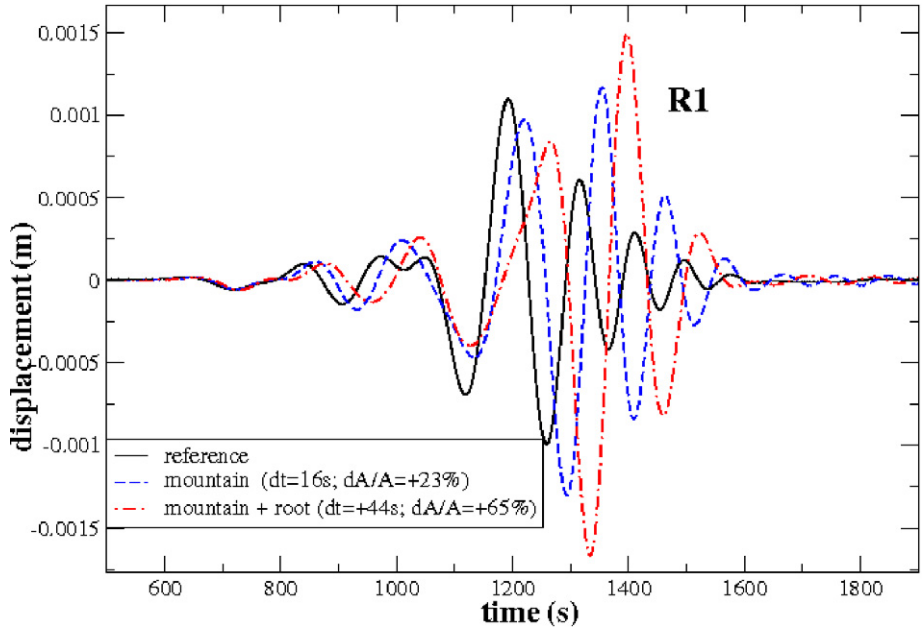

(a)

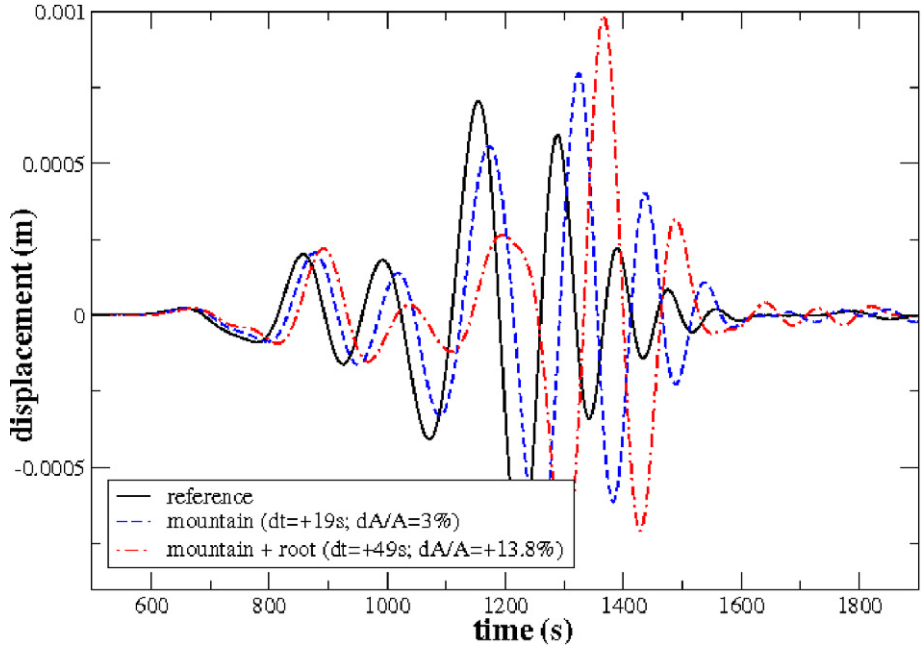

(b)

Fig. 5. Comparison of the effects obtained in the presence of a mountain with and without a compensating root. The receiver is at the center of the relief. The vertical component is presented in (a), the radial one in (b).

der to examine this hypothesis, we change the martian velocity model by considering a mean value for the crust thickness of 50 km. The signal distortion in this case is indeed more important as can be seen in Fig. 8.

5. Discussion and conclusions

By using the spectral element–modal solution method, effects of crust thickness variation upon seismograms has been investigated. Due to limited computational resources, that study was limited to very long periods (above 80 s). We show that elevations in the topography of the surface tend to decrease the apparent travel-time of seismic waves when the presence of basins tend to increase it only by geometrical effects. Presence of reliefs change also the amplitude of the arriving waves. These effects are larger when the surface topography is compensated by a mirror-image topography for the "Moho." Gravity studies suggest that the crust of Mars is indeed in an isostasy state. We show that apparent velocity anomalies up to 1% can be induced by only the geometrical flexure of the surface and of the "Moho." 1% anomalies are of the same order than anomalies induced by the upper mantle heterogeneities in the Earth. It is

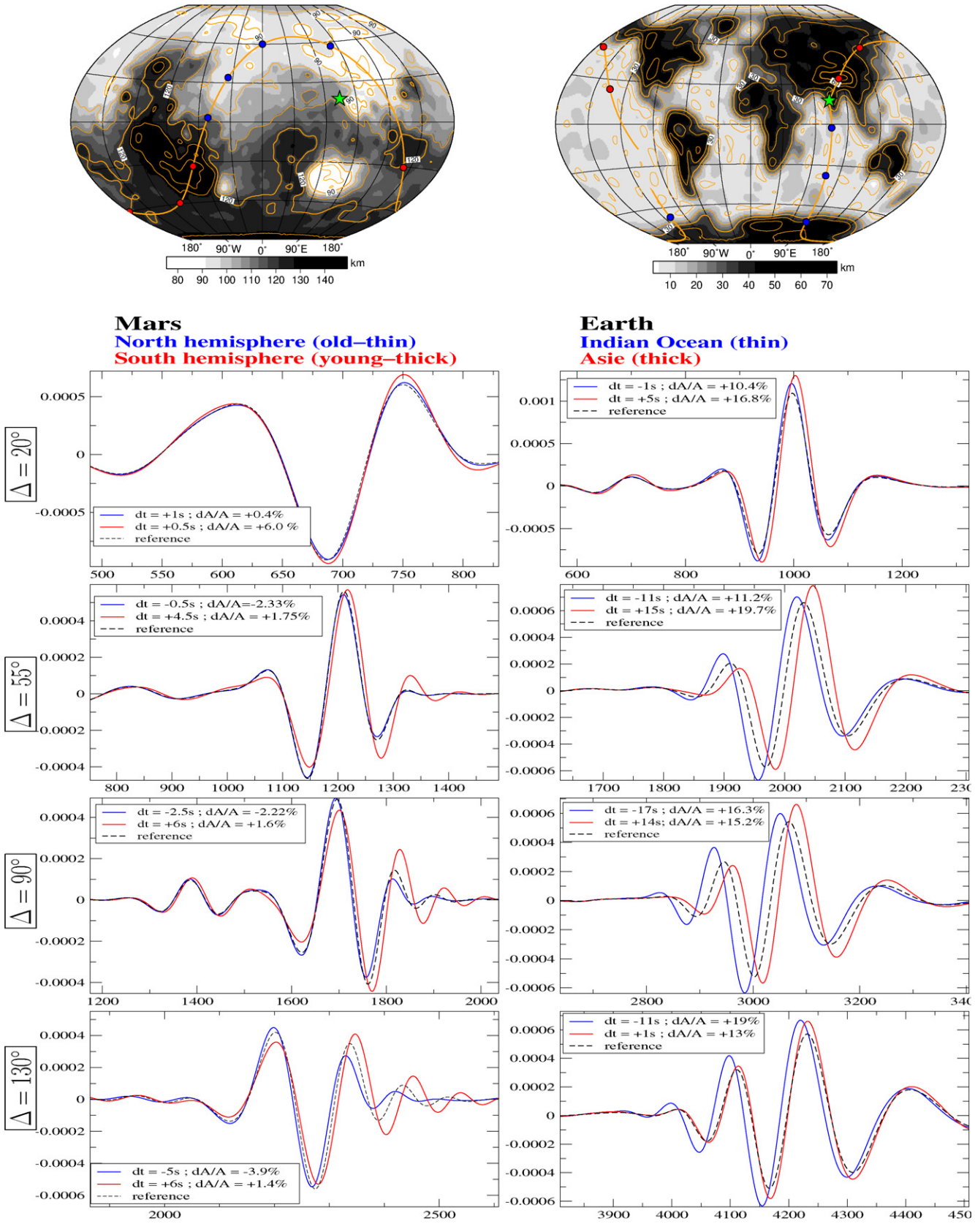

Fig. 6. Comparison between the case of Mars and of the Earth of the effects of crust thickness variations on the first train of Rayleigh waves. The effects in terms of time delays are similar between the north thin hemisphere of Mars and the Indian oceanic plate and between the south thick hemisphere and the Himalayan relief. The reference traces have been computed in perfectly sphericals models (no topography) using the modal solution. Each trace is represented with time in seconds on the x-axis and displacement in m on the y-axis.

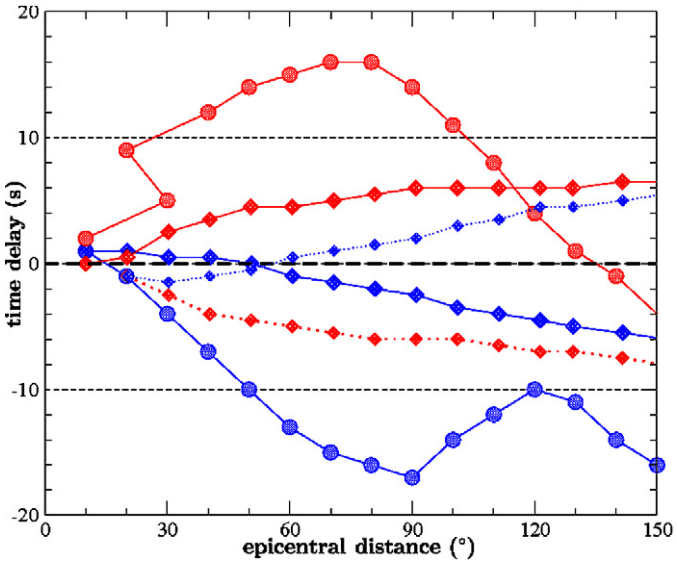

(a)

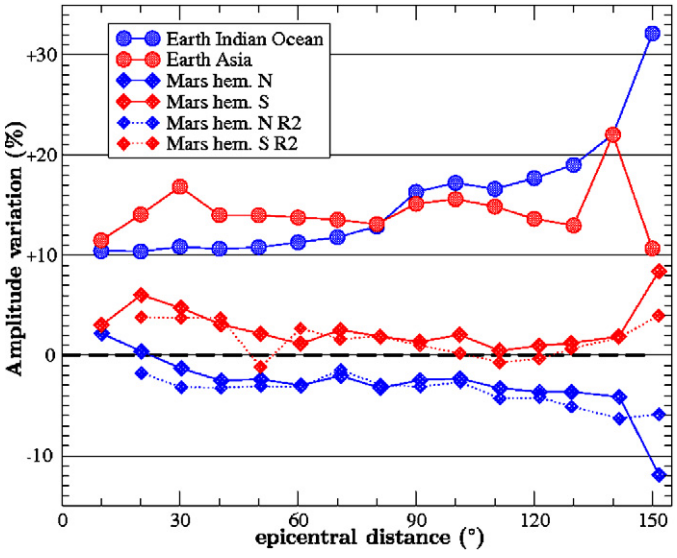

(b)

Fig. 7. Quantification of the distorsion of surface waves in the two realistic models of the Earth and Mars. The effects on the Earth are more important than on Mars surely because crust thickness variation are relatively more important in the case of the Earth. Notice that the dichotomy of the shape of the martian crust is clearly visible on the curves. By traveling across the thin north hemisphere, the surface wave are characterized by earlier arrivals and a decrease of their amplitude. When they reach the south hemisphere, they become the R2 train and they start losing their advance. As for the amplitude, the receivers on the South hemisphere systematically show larger amplitude than the ones for the North hemisphere for the R1 and the R2 trains.

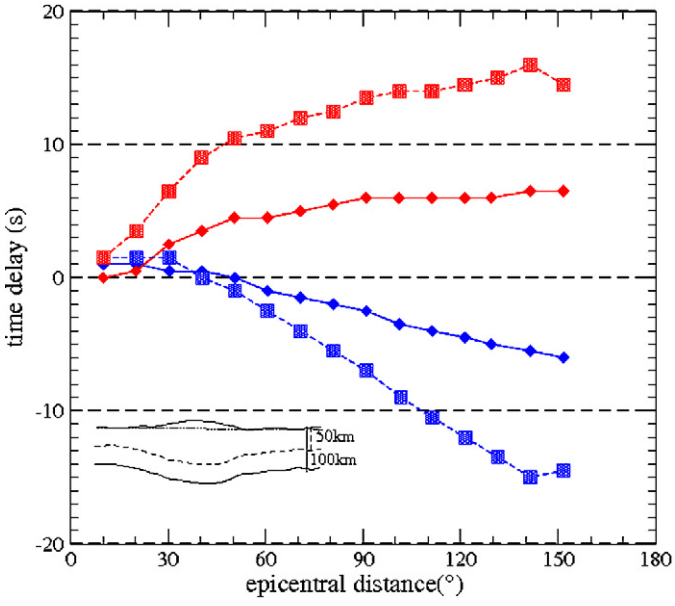

(a)

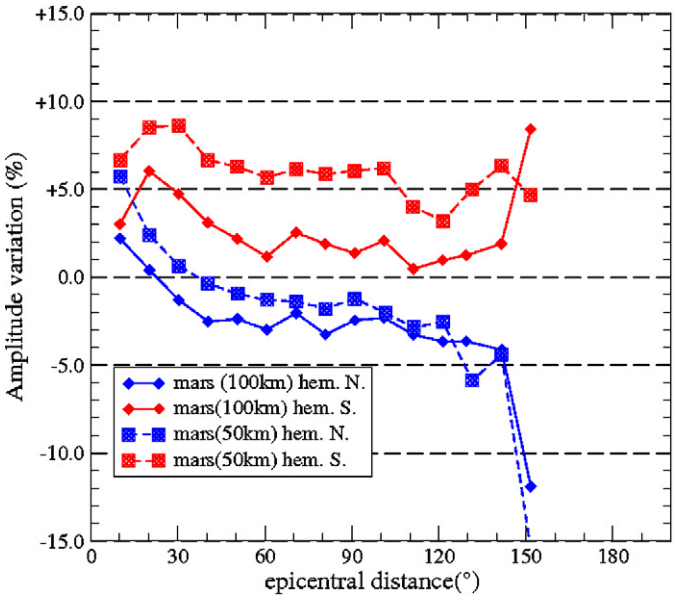

(b)

Fig. 8. Influence of the crust thickness on the distortion of the seismic waves. Results for two models of Mars with a mean crustal thickness of 100 and 50 km, respectively, are compared. The effects of the surface topography (which is the same in the two cases), are larger when the crust is thinner because of crust is relatively more deformed is this case.

worth remembering that some tomography studies did image supposed plumes below the Tibet plateau because no topography correction were performed. These low velocity zones disappear when the correct structure of the crust was taken into account (Griot et al., 1998). Narrower reliefs, such as the Olympus Mount, produces a seismic signal whose behavior is similar to the one induced by a scatterer: new diffracted phases appear in the seismic signal when time delay of arrival time of classical waves have a tendency to vanish after a propagation of several wavelengths from the relief.

Because Mars exhibits a spectacular surface topography, we expected that effect of topography would have been larger for Mars than for the Earth. It is the contrary. Seismograms computed in a realistic Earth model show larger distortion relatively to the spherical reference model than in the Mars case. It is because the relative variations of the crust thickness are larger for the Earth (absolute amplitude for the topography of 10 km for a mean crust thickness of 35 km for the Earth to be compared to an amplitude of 27 km for a mean of 100 km for Mars). When changing the Mars model for a thinner crust with a mean thickness of 50 km, effects by the topography on Mars

seismograms becomes of the same order when not larger than what is observed on the Earth. Nevertheless, due to the likely small number of the first seismic stations on Mars, specially in the early-stage of the future Mars seismic network, it is of importance to be able to isolate correctly crust and upper mantle effects on seismograms.

Acknowledgments

This work was supported by the department of seismology of the Institut de Physique du Globe of Paris, by the seismological laboratory of the California Institute of Technology, Pasadena. It was done in collaboration with the Jet Propulsion Laboratory, Pasadena. The simulations were performed on the clusters of the department of numerical modelization of the IPGP. We would like to thank Renee Bulow and an anonymous reviewer for their useful comments on this manuscript.

References

Anderson, D.L., Duennebier, F.K., Latham, G.V., Toksoz, M.F., Kovach, R.L., Knight, T.C.D., Lazarewicz, A.R., Miller, W.F., Nakamura, Y., Sutton, G., 1976. The Viking seismic experiment. Science 194 (4271), 1318–1321.

Anderson, D.L., Miller, W.F., Latham, G.V., Nakamura, Y., Toksoz, M.N., Dainty, A.M., Duennebier, F.K., Lazarewicz, A.R., Kovach, R.L., Knight, T.C.D., 1977. Seismology on Mars. J. Geophys. Res. 82 (28), 4524–4546.

Banerdt, W.B., 1986. Support of long-wavelength loads on Venus and implications for internal structure. J. Geophys. Res. 91 (B1), 403–419.

Belleguic, V., Lognonné, P., Wieczorek, M., 2005. Constraints on the martian lithosphere from gravity and topography data. J. Geophys. Res. Planets 110 (E11), doi:10.1029/2005JE002437. E11005.

Biele, J., Ulamec, S., Spohn, T., Mimoun, D., Lognonné, P., the GEP team, 2007. GEP–ExoMars: A Geophysics and Environment Observatory on Mars. Lunar Planet. Sci. XXXVIII.

Bills, B.G., Neumann, G.A., Smith, D.E., Zuber, M.T., 2005. Improved estimate of tidal dissipation within Mars from MOLA observations of the shadow of Phobos. J. Geophys. Res. Planets 110 (E7). E07004.

Capdeville, Y., 2000. Méthode couplée éléments spectraux–solution modale pour la propagation d'ondes dans la Terre à l'échelle globale. Ph.D. thesis, Institut de Physique du Globe de Paris.

Capdeville, Y., Chaljub, E., Vilotte, J.-P., Montagner, J.-P., 2003. Coupling the spectral element method with a modal solution for elastic wave propagation in global Earth models. Geophys. J. Int. 152 (1), 34–67.

Capdeville, Y., Larmat, C., Vilotte, J.-P., Montagner, J.-P., 2002. A new coupled spectral element and modal solution method for global seismology: A first application to the scattering induced by a plume-like anomaly. Geophys. Res. Lett. 29 (9), 32. .1–32.4.

Chaljub, E., 2000. Modélisation numérique de la propagation d'ondes simiques en géométrie sphérique: Application à la sismologie globale. Ph.D. thesis, Institut de Physique du Globe de Paris.

Chaljub, E., Capdeville, Y., Vilotte, J.-P., 2003. Solving elastodynamics in a fluid–solid heterogeneous sphere: A parallel spectral element approximation on non-conforming grids. J. Comput. Phys. 187 (2), 457–491.

Golombek, M.P., 2002. A revision of Mars seismicity from surface faulting. Lunar Planet. Sci. XXXIII.

Golombek, M.P., Banerdt, W.B., Tanaka, K.L., Tralli, D.M., 1992. A prediction of Mars seismicity from surface faulting. Science 258 (5084), 979–981.

Griot, D.-A., Montagner, J.-P., Tapponnier, P., 1998. Phase velocity structure from Rayleigh and Love waves in Tibet and its neighboring regions. J. Geophys. Res. 103 (B9), 21215–21232.

gtopo30, Documentation by US Geological Survey. http://edc.usgs.gov/products/elevation/gtopo30/README.html.

Harri, A.-M., Marsal, O., Lognonné, P., Leppelmeier, G.W., Spohn, T., Glassmeier, K.-H., Angrilli, F., Banerdt, W.B., Barriot, J.-P., Bertaux, J.-L., Berthelier, J.J., Calcutt, S., Cerisier, J.C., Crisp, D., Dehant, V., Giardini, D., Jaumann, R., Langevin, Y., Menvielle, M., Musmann, G., Pommereau, J.P., Pippo, S.D., Guerrier, D., Kumpulainen, K., Larsen, S., Mocquet, A., Polkko, J., Runavot, J., Schumacher, W., Siili, T., Simola, J., Tillman, J.E., the Netlander Team, 1999. Network science landers for Mars. Adv. Space Res. 23 (11), 1915–1924.

Komatitsch, D., 1997. Méthodes spectrales et éléments spectraux pour l'équation de l'élastodynamique 2D et 3D en milieu hétérogène. Ph.D. thesis, Institut de Physique du Globe de Paris.

Lognonné, P., 2005. Planetary seismology. Annu. Rev. Earth Planet. Sci. 33, 571–604. http://dx.doi.org/10.1146/annurev.earth.33.092203.122604.

Lognonné, P., Mosser, B., 1993. Planetary seismology. Surv. Geophys. 14 (3), 239–302.

Lognonné, P., Johnson, C., 2007. Planetary Seismology. In: Treatise in Geophysics. Elsevier, Amsterdam. Section 10.04.

Lognonné, P., Gagnepain-Beyneix, J., Banerdt, W.B., Cacho, S., Karczewski, J.F., Morand, M., 1996. Ultra-broad band seismology on InterMarsnet. Planet. Space Sci. 44 (11), 1237–1249.

Lognonné, P., Zharkov, V.N., Karczewski, J.F., Romanowicz, B., Menvielle, M., Poupinet, G., Brient, B., Cavoit, C., Desautez, A., Dole, B., Franqueville, D., Gagnepain-Beyneix, J., Richard, H., Schibler, P., Striebig, N., 1998. The seismic OPTIMISM experiment. Planet. Space Sci. 46 (6–7), 739–747.

Lognonné, P., Giardini, D., Banerdt, B., Gagnepain-Beyneix, J., Mocquet, A., Spohn, T., Karczewski, J.F., Schibler, P., Cacho, S., Pike, W.T., Cavoit, C., Desautez, A., Favède, M., Gabsi, T., Simoulin, L., Striebig, N., Campillo, M., Deschamp, A., Hinderer, J., Lévéque, J.J., Montagner, J.-P., Rivéra, L., Benz, W., Breuer, D., Defraigne, P., Dehant, V., Fujimura, A., Mizutani, H., Oberst, J., 2000. The Netlander very broadband seismometer. Planet. Space Sci. 48 (12–14), 1289–1302.

Lognonné, P., Gagnepain-Beyneix, J., Chenet, H., 2003. A new seismic model of the Moon: Implications for structure, thermal evolution and formation of the Moon. Earth Planet. Sci. Lett. 211 (1–2), 27–44.

Malin, M.C., Edgett, K.S., 2001. Mars Global Surveyor Mars Orbiter Camera: Interplanetary cruise through primary mission. J. Geophys. Res. 106 (E10), 23429–23570.

McLennan, S.M., 2001. Crustal heat production and the thermal evolution of Mars. Geophys. Res. Lett. 28 (21), 4019–4022.

Mocquet, A., 1999. A search for the minimum number of stations needed for seismic networking on Mars. Planet. Space. Sci. 47 (3–4), 397–409.

Mocquet, A., Vacher, P., Grasset, O., Sotin, C., 1996. Theoretical seismic models of Mars: The importance of the iron content of the mantle. Planet. Space Sci. 44 (11), 1251–1268.

Nimmo, F., Stevenson, D.J., 2001. Estimates of martian crustal thickness from viscous relaxation of topography. J. Geophys. Res. 106 (E3), 5085–5098.

Paolucci, R., Faccioli, E., Maggio, F., 1999. 3D response analysis of an instrumented hill at Matsuzaki, Japan, by a spectral method. J. Seismol. 3 (2), 191–209.

Ricard, Y., Nataf, H.C., Montagner, J.-P., 1996. The three-dimensional seismological model a priori constrained: Confrontation with seismic data. J. Geophys. Res. 101 (B4), 8457–8472.

Smith, D.E., Zuber, M.T., 1996. The shape of Mars and the topographic signature of the hemispheric dichotomy. Science 271 (5246), 184–188.

Smith, D.E., Zuber, M.T., Frey, H.V., Garvin, J.B., Head, J.W., Muhleman, D.O., Pettengill, G.H., Phillips, R.J., Solomon, S.C., Zwally, H.J., Banerdt, W.B., Duxbury, T.C., Golombek, M.P., Lemoine, F.G., Neumann, G.A., Rowlands, D.D., Aharonson, O., Ford, P.G., Ivanov, A.B., Johnson, C.L., McGovern, P.J., Abshire, J.B., Afzal, R.S., Sun, X.L., 2001. Mars Orbiter Laser Altimeter: Experiment summary after the first year of global mapping of Mars. J. Geophys. Res. 106 (E10), 23689–23722.

Snieder, R., 1986. Phase speed perturbations and three-dimensional scattering effects of surface waves due to topography. Bull. Seismol. Soc. Am. 76 (5), 1385–1392.

Sohl, F., Spohn, T., 1997. The interior structure of Mars: Implications from the SNC meteorites. J. Geophys. Res. 102 (E1), 1613–1635.

Spohn, T., Sohl, F., Breuer, D., 1998. Mars. Astron. Astrophys. Rev. 8 (3), 181–236.

Turcotte, D.L., 1987. A fractal interpretation of topography and geoid spectra on the Earth, Moon, Venus, and Mars. J. Geophys. Res. Solid Earth Planets 92 (B4), E597–E601.

Turcotte, D.L., Shcherbakov, R., Malamud, B.D., Kucinskas, A.B., 2002. Is the martian crust also the martian elastic lithosphere? J. Geophys. Res. Planets 107 (E11), 1.1–1.20.

Verhoeven, O., Rivoldini, A., Vacher, P., Mocquet, A., Choblet, G., Menvielle, M., Dehant, V., Hoolst, T.V., Sleewaegen, J., Barriot, J.-P., Lognonné, P., 2005. Interior structure of terrestrial planets: Modeling Mars' mantle and its electromagnetic, geodetic, and seismic properties. J. Geophys. Res. Planets 110 (E4) E04009.

Wieczorek, M.A., Zuber, M.T., 2004. Thickness of the Martian crust: Improved constraints from geoid-to-topography ratios. J. Geophys. Res. Planets 109 (E1), E01009.

Yoder, C.F., Konopliv, A.S., Yuan, D.N., Standish, E.M., Folkner, W.M., 2003. Fluid core size of Mars from detection of the solar tide. Science 300 (5617), 299–303.

Zharkov, V.N., Gudkova, T.V., 1997. On the dissipative factor of the martian interiors. Planet. Space Sci. 45 (4), 401–407.

Zhong, S.J., Zuber, M.T., 2001. Degree-1 mantle convection and the crustal dichotomy on Mars. Earth Planet. Sci. Lett. 189 (1–2), 75–84.

Zuber, M.T., Solomon, S.C., Phillips, R.J., Smith, D.E., Tyler, G.L., Aharonson, O., Balmino, G., Banerdt, W.B., Head, J.W., Johnson, C.L., Lemoine, F.G., McGovern, P.J., Neumann, G.A., Rowlands, D.D., Zhong, S., 2000. Internal structure and early thermal evolution of Mars from Mars Global Surveyor topography and gravity. Science 287 (5459), 1788–1793.